Reduction of Influence of Variation in Center Frequencies of RF Echoes on Estimation of Artery-Wall Strain

Hideyuki Hasegawa and Hiroshi Kanai, *Member, IEEE*

***Abstract*—Atherosclerotic change of the arterial wall leads to a significant change in its elasticity. For assessment of elasticity, measurement of arterial wall deformation is required. For motion estimation, correlation techniques are widely used, and we have developed a phase-sensitive correlation method, namely, the phased-tracking method, to measure the regional strain of the arterial wall due to the heartbeat. Although phase-sensitive methods using demodulated complex signals require less computation in comparison with methods using the correlation between RF signals or iterative methods, the displacement estimated by such phase-sensitive methods are biased when the center frequency of the RF echo apparently varies. One of the reasons for the apparent change in the center frequency would be the interference of echoes from scatterers within the wall. In the present study, a method was introduced to reduce the influence of variation in the center frequencies of RF echoes on the estimation of the artery-wall strain when using the phase-sensitive correlation technique. The improvement in the strain estimation by the proposed method was validated using a phantom. The error from the theoretical strain profile and the standard deviation in strain estimated by the proposed method were 12.0% and 14.1%, respectively, significantly smaller than those (23.7% and 46.2%) obtained by the conventional phase-sensitive correlation method. Furthermore, in the preliminary *in vitro* experimental results, the strain distribution of the arterial wall well corresponded with pathology, i.e., the region with calcified tissue showed very small strain, and the region almost homogeneously composed of smooth muscle and collagen showed relatively larger strain and clear strain decay with respect to the radial distance from the lumen.**

I. Introduction

Pathological change of the arterial wall due to atherosclerosis leads to a significant change in its mechanical properties [1], [2]. Most conventional methods for noninvasive measurement of elasticity are based on measurement of the pulse wave velocity (PWV) [3]–[6] or that of the change in diameter [7]–[10]. Although these methods are useful in terms of their ability to assess the vascular elasticity noninvasively, the spatial resolution in elasticity measurement is limited to the propagating distance of the pulse wave or the entire circumference.

Manuscript received February 3, 2007; accepted February 24, 2008.

This work was supported by the Ministry of Education, Science, Sports and Culture and was partly supported by the Suzuken Memorial Foundation.

H. Hasegawa and H. Kanai are with Department of Electronic Engineering, Graduate School of Engineering, Tohoku University, Sendai, Japan (email: hasegawa@us.ecei.tohoku.ac.jp).

Digital Object Identifier 10.1109/TUFFC.884

Elastography was introduced by Ophir *et al.* to measure the strain distribution of biological tissue by cross-correlating 2 RF signals before and after deformation [11]–[14]. Elastography was applied to strain imaging of the arterial wall with intravascular ultrasonography (IVUS), namely, intravascular elastography [15], [16]. In the cited studies, the elasticity distribution of coronary atherosclerotic plaque was obtained by the measured displacement distribution in the radial direction. This measured elasticity distribution was compared with the pathological image, and the results suggested the potential for tissue characterization of atherosclerotic plaque by measurement of its elasticity.

As a transcutaneous approach, the displacement and strain around carotid atherosclerotic plaque during one cardiac cycle have been measured using tissue Doppler imaging [17]. The inhomogeneity of displacements measured upstream and downstream of atherosclerotic plaque suggests that artery-wall motion has potential for use in the evaluation of plaque vulnerability. Furthermore, some research studies on noninvasive vascular elastography have been conducted [18]–[20]. In most of the above-mentioned methods, a correlation-based technique is used for the estimation of the displacement and strain of the arterial wall [15]–[18], [21]. Also, in recent years, iterative methods have been introduced for estimating 2-D displacement [19], [22].

We have been studying the measurement of the displacement and radial strain (change in thickness) of the arterial wall based on the phase-sensitive correlation technique and have developed the phased-tracking method [23]–[27]. Elasticity images of the human carotid artery have been obtained based on the measured strain distribution, and the potential for transcutaneous tissue characterization has been shown by classification of elasticity images using elasticity reference data obtained by *in vitro* experiments [28]–[31].

The phase-sensitive correlation method using a demodulated complex signal, which was first introduced by Kasai *et al.* for blood flow measurement [32], requires less computation in comparison with the cross-correlation between RF signals. Methods based on the cross-correlation between RF signals can estimate displacement larger than half of the wavelength of ultrasound, but such estimation requires calculation of correlation functions at multiple lags between RF signals in 2 frames. On the other hand, phase-sensitive correlation methods estimate displacement less than half of the wavelength, but require calculation of

only one complex correlation function at no lag between demodulated complex signals in 2 frames. The displacement of an object can be estimated using phase-sensitive methods by keeping the frame rate sufficiently high so that the displacement between 2 frames becomes less than half of the wavelength of ultrasound. However, the displacements estimated by phase-sensitive methods are biased when the center frequency of the RF echo apparently varies. One of the reasons for the apparent change in center frequency would be the interference of echoes from scatterers within the wall. The center frequency could be apparently changed depending on the scatterer spacing.

Konofagou *et al.* proposed a method to estimate tissue strain from the shift of the centroids in power spectra of RF echoes by assuming that the change in center frequency is proportional to the magnitude of strain. As described in [33], [34], this method is robust when the decorrelation of RF signals in 2 different frames is significant due to a large strain of up to 10% between frames. However, the accuracy of this method is worse than those of methods based on cross-correlation of RF signals when the signal correlation is assured.

In methods based on the cross-correlation of RF signals in 2 frames, companding, termed temporal stretching, is applied to the RF signals before correlating them to compensate for the change in center frequency distributions between 2 frames (called scaling) [12], [35]–[42]. Such difference between the center frequency distributions in 2 frames is not negligible when the strain that arises between 2 frames is large because a large deformation significantly changes the spacing of scatterers. Although the center frequency "difference" between 2 frames is compensated by companding, the center frequency distributions themselves are not spatially homogeneous, even after the application of companding. Nevertheless, such methods yield unbiased displacement estimates by compensating for only the center frequency difference between 2 frames [21] because the displacement estimation by the cross-correlation between RF signals does not require knowledge of the center frequency. However, as described in [21], such methods require considerable computation because both the scale factor in companding and time delay between RF signals must be determined.

In the phase-sensitive correlation-based methods, a subsample small displacement between 2 consecutive frames is estimated using the phase of the complex correlation function. In these methods, the center frequency distributions in 2 consecutive frames are assumed to be the same when the frame rate is sufficiently high and the deformation between 2 consecutive frames is small. Therefore, companding is not applied. However, knowledge of the center frequency at each location is necessary to obtain an unbiased displacement estimate using the phase of the complex correlation function. Although Loupas *et al.* proposed a method for estimating the center frequency distribution by correlation of the demodulated complex signals [43], [44], center frequency distributions in 2 frames are still assumed to be the same.

In this study, a new method using the phase-sensitive correlation technique, which does not require the assumption that center frequency distributions in 2 different frames are the same, was examined with the aim of reducing the influence of center frequency variation on the estimation of artery-wall strain. The improvement of accuracy by the proposed method was validated using a cylindrical phantom. Furthermore, preliminary *in vitro* experimental results were obtained and are herein presented.

II. Principles

A. Conventional Phase-Sensitive Correlation Method for Estimating Displacement Distribution in the Arterial Wall

The ultrasonic beam scans I (= 46 in this study) positions along the longitudinal direction of the artery. As shown in Fig. 1, with respect to each beam position i (= 1,2,...,I), RF pulses are transmitted with a time interval T from an ultrasonic probe, and the echo reflected by the arterial wall is received by the same probe. By referring to a B-mode or M-mode image constructed based on the received RF echoes, the depths, $x_1(0)$ and $x_{M_T}(0)$ (corresponding to the distances from the probe), of the lumen-intima and media-adventitia boundaries of the posterior wall are manually assigned in the initial frame, where M_T is the number of sampled points between these assigned boundaries. Depth $x_m(n)$ at the m-th sampled points (m = 1,2,...,M_T) in the nth frame is defined as follows:

$$x_m(n) = x_1(n) + (m-1)\cdot\Delta X, \quad (m = 1,2,...,M_T) \tag{1}$$

where $\Delta X = c_0/(2f_s)$ (f_s: sampling frequency) is the interval of sampled points in the direction of depth. After depths $x_1(0)$ and $x_{M_T}(0)$ in the initial frame $n = 0$ are manually assigned, the displacements $\{u_m(n)\}$ (m = 1,2,...,M_T) at multiple points along an ultrasonic beam are obtained by estimating the instantaneous displacement, $\{\Delta u_m(n)\}$, between nth and $(n+1)$th frames (n = 0,1,2,...,N) at the respective points m (= 1,2,...,M_T) as described below.

Let us define the RF signal at depth x and beam position i in the nth frame by $s_i(n;x)$. The instantaneous displacement, $\Delta u_m(n)$, at $x_m(n)$ between the nth and $(n+1)$th frames (corresponding to the average velocity between 2 frames) is estimated based on the time delay, $\Delta\tau_m(n)$, between RF signals, $s_i(n;x)$ and $s_i(n+1;x)$, at $x = x_m(n)$ because displacement $\Delta u_m(n)$ between the nth and $(n+1)$th frames is expressed by $\Delta u_m(n) = c_0\Delta\tau_m(n)/2$, where c_0 is the speed of sound [23], [32]. Time delay $\Delta\tau_m(n)$ at the mth sampled point is related to the phase change $\Delta\theta_m(n)$ of $s_i(n+1;x)$ from $s_i(n;x)$ as follows:

$$\Delta\tau_m(n) = \frac{\Delta\theta_m(n)}{2\pi f_{c,m}(n)}, \tag{2}$$

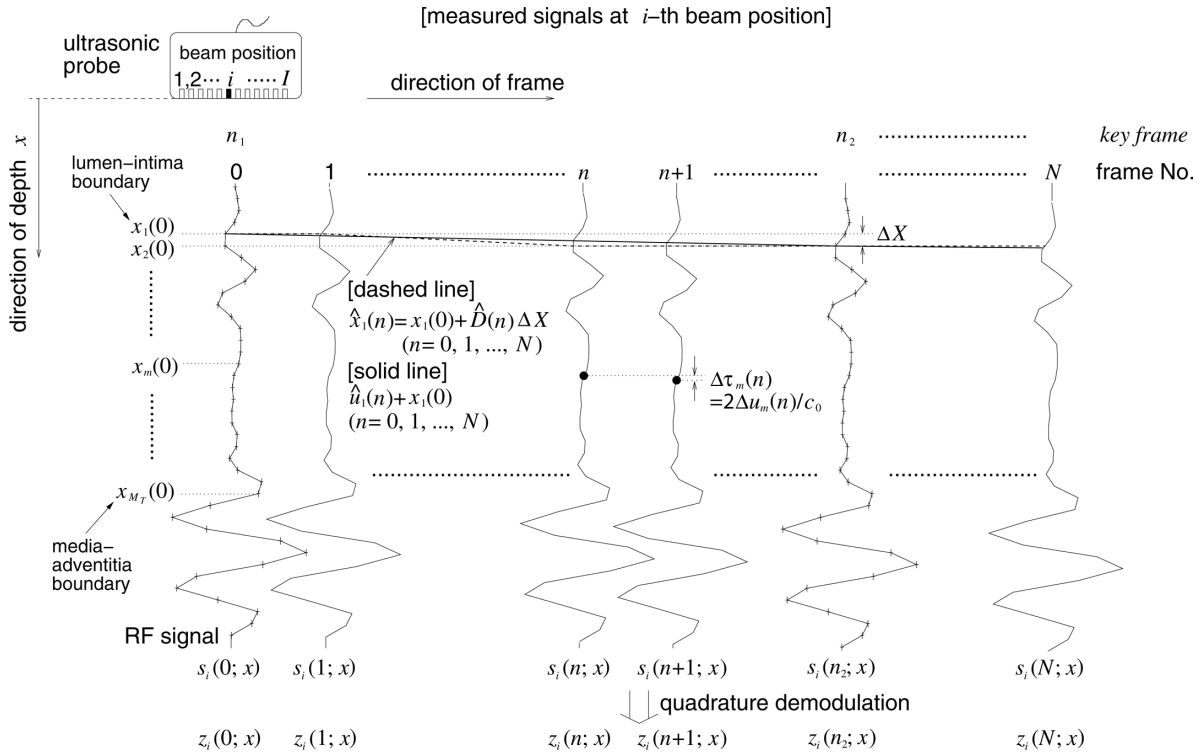

Fig. 1. Illustration of variables.

where $f_{c,m}(n)$ is the center frequency of the RF echo at depth $x_m(n)$ in the nth frame. As described in Section II-B, center frequency $f_{c,m}(n)$ is not spatially constant along the ultrasonic beam and temporally varies because the frame is different. Using the quadrature demodulated signal, $z_i(n;x)$, of $s_i(n;x)$, phase shift $\Delta\theta_m(n)$ between 2 frames at depth $x_m(n)$ can be estimated by the complex correlation $r_{m,n}(m',n')$ as follows [32]:

$$r_{m,n}(m',n') = \sum_{j=i-I_{av}}^{i+I_{av}} \sum_{l=0}^{M_c-1} z_j^*(n; x_m(n) + l \cdot \Delta X) \cdot z_j(n+n'; x_m(n) + (l+m') \cdot \Delta X), \quad (3)$$

where * represents the complex conjugate and $r_{m,n}(m',n')$ defines the complex correlation function with lags, m' and n', in the directions of depth and frame, respectively. Although the correlation function is usually normalized by the average amplitude of the complex signal in the correlation window, normalization was not applied in this study because only the phase of the complex correlation function was used for estimation of the displacement. The number of sampled points in the direction of depth used for calculating correlation is defined by M_c, and the correlation window extends from the mth point to the $(m + M_c - 1)$th point because the leading edge of the echo from the point of interest (= mth points) should correspond to mth point. Phase angle $\angle r_{m,n}(0,1)$ of $r_{m,n}(0,1)$ corresponds to the phase shift $\Delta\theta_m(n)$ between RF echoes in 2 consecutive frames [32], where $r_{m,n}(0,1)$ means the correlation between signals at the same depth ($m' = 0$) in 2 consecutive frames ($n' = 1$). In blood flow measurement using the complex correlation, the correlation function $r_{m,n}(m',n')$ is temporally averaged in the direction of the frame. This can be done because the RF signals are acquired at a very high frame rate (several kHz) in the measurement of blood flow. Although the frame rate in this study (286 Hz) was higher than that in conventional B-mode imaging (at most 60 Hz), it was much lower than that in blood flow measurement, and temporal averaging in the direction of the frame was not applied in (3).

In this study, a 2-D kernel was used in calculation of the complex correlation function to reduce the variance in the estimated displacement distribution in the arterial wall. The 2-D kernel was used even when the displacement was estimated based on the conventional methods described in this section to compare the estimated displacements with those by the proposed method. The phase angle $\angle r_{m,n}(0,1)$ represents the spatially averaged phase shift of RF echoes in the correlation window consisting of (M_c samples) $\times$ ($(2I_{av} + 1)$ beam positions). In this study, I_{av} was set to 1 because the number $(2I_{av} + 1)$ of averaging (beam positions) is significantly increased from 1 to 3 (200% increase) when I_{av} changes from 0 to 1, but the number $(2I_{av} + 1)$ is not increased so much (67%: $I_{av} = 1 \rightarrow 2$, 40%: $I_{av} = 2 \rightarrow 3$) when I_{av} is further increased. In addition, a larger I_{av} worsens the lateral spatial resolution.

In the conventional phase-sensitive correlation method, using the estimated phase shift, $\widehat{\Delta\theta}_m(n) = \angle r_{m,n}(0,1)$, instantaneous displacement $\Delta u_m(n)$ between 2 consecutive frames is obtained as follows:

$$\widehat{\Delta u}_m(n) = \frac{c_0 \widehat{\Delta\theta}_m(n)}{4\pi f_{c,m}(n)} \approx \frac{c_0 \widehat{\Delta\theta}_m(n)}{4\pi f_{dem}} = \frac{c_0}{4\pi f_{dem}} \angle r_{m,n}(0,1). \tag{4}$$

In (4), knowledge of the center frequency $f_{c,m}(n)$ is necessary to obtain an unbiased estimate. It is, however, unknown. Therefore, in conventional phase-sensitive correlation methods, the frequency of the reference sinusoid, f_{dem}, in the quadrature demodulation is used as the frequency term in the denominator of (4), whereas it should be the actual center frequency $f_{c,m}(n)$.

The accumulated displacement, $u_m(n)$, is obtained by accumulating the estimated instantaneous displacement $\Delta u_m(n)$ between 2 consecutive frames as follows:

$$\hat{u}_m(n+1) = \hat{u}_m(n) + \widehat{\Delta u}_m(n) \qquad (u_m(0) = 0). \tag{5}$$

Depth $x_1(n)$ of the first point (luminal interface of the posterior wall) in the nth frame is determined by accumulated displacement $\hat{u}_1(n)$ as follows:

$$\hat{x}_1(n) = x_1(0) + \hat{D}(n) \cdot \Delta X, \tag{6}$$

where $\hat{D}(n)$ is an integer that satisfies $\min_{D(n)} |\hat{u}_1(n) - D(n) \cdot \Delta X|$ because the position of a correlation window is set depending on the spacing of the sampled points. For other points $\{m\}$, their depths $\{x_m(n)\}$ in the nth frame are determined by (1).

B. Modified Method for Estimation of Displacement Distribution

Fig. 2(a) shows a B-mode image of the phantom used in this study. The RF echo along the white vertical line in Fig. 2(a) is shown in Fig. 2(b). As can be seen in Fig. 2(b), the center frequency is not constant along the ultrasonic beam. This change in center frequency does not occur due to the well-known frequency dependent attenuation of ultrasound because the center frequency in a deep region—region B in Fig. 2(b)—is higher than that in a shallow region (region A).

When a target contains multiple scatterers within the duration of an ultrasonic pulse, interference between echoes from these scatterers occurs. An ultrasonic pulse has a certain frequency bandwidth, and thus such interference could be one of the reasons for the apparent change in center frequency (see the appendix). This subsection describes the displacement estimation method proposed in this study for reduction of the influence of center frequency variation.

The modified method comprises 2 main procedures: 1) estimation of displacement distribution in the arterial wall with tracking of the global motion of the arterial wall and 2) error reduction of the estimated displacement distribution using a newly proposed function.

1. Estimation of Displacement Distribution in Arterial Wall with Tracking of Global Motion: In conventional phase-sensitive correlation methods, the center frequency distributions in 2 different frames are assumed to be the same. Therefore, it is desired that the frame rate be as high as possible so that the deformation of the arterial wall becomes negligible, and thus the displacement should be estimated for every 2 consecutive frames.

On the other hand, the modified method does not require the above assumption. Therefore, the displacement distribution in the arterial wall need not be estimated for every 2 consecutive frames. Thus, several key frames are sparsely assigned, and the displacement distribution between 2 consecutive key frames is estimated. This procedure significantly reduces the number of calculations because the displacement of the arterial wall between 2 consecutive frames (4.2 μm) is smaller than the spacing of sampled points (19.25 μm), and thus there are multiple frames between 2 consecutive key frames, where the displacement of 4.2 μm is derived from the mean wall velocity of 1.2 mm/s during one cardiac cycle (measured in the carotid artery of a healthy subject) at a frame rate of 286 Hz. In this procedure, only the displacement at the luminal boundary is estimated using the conventional phase-sensitive correlation method described in Section II-A for every 2 consecutive frames so that the correlation window follows the position of the arterial wall (tracking of global motion).

Details of the above procedures are as follows: In this study, the global motion of the arterial wall is tracked using the displacement $u_1(n)$ of the luminal boundary estimated by the conventional method described in Section II-A because the echo from the luminal interface is usually dominant in comparison with those from scatterers in the wall and is robust against interference. The displacement $u_1(n)$ of echo from the luminal interface is estimated for every 2 frames at a high frame rate of 286 Hz. Therefore, the instantaneous displacement $\Delta u_1(n)$ between 2 consecutive frames is less than the spacing ΔX of the sampled points in the direction of depth x.

Fig. 3 shows an example of the accumulated displacement $u_1(n)$ at the luminal interface of the phantom used in this study. In this study, several key frames are defined as shown in Fig. 3. The frame number of the kth key frame is denoted by n_k, and key frames are set so that the difference between the accumulated displacement $u_1(n_k + 1)$ in the $(k + 1)$th key frame and that $u_1(n_k)$ in the kth key frame reaches spacing ΔX of the sampled points. Then, the global motion of the wall is compensated by shifting the RF signal in the $(k + 1)$th key frame by ΔX of the sampled points before calculating the phase shift of RF echoes to obtain displacement $\Delta u_m(n_k)$ between 2 consecutive key frames. This is done by setting lags m' and n' in (3) to be $\hat{D}(n_{k+1}) - \hat{D}(n_k)$ and $n_{k+1} - n_k$, respectively, as follows:

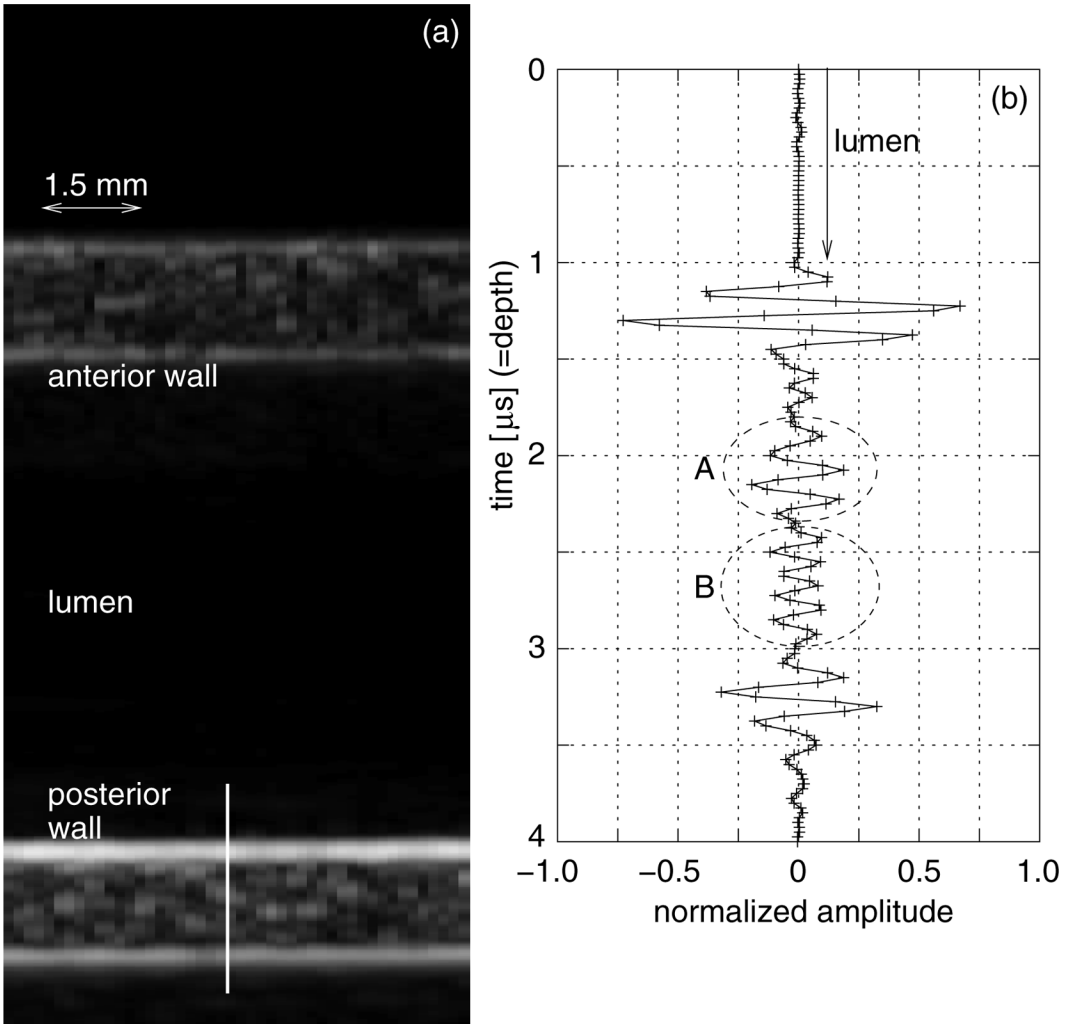

Fig. 2. (a) B-mode image of the phantom used in this study and (b) waveform of received RF echo along white vertical line in (a).

$$\widehat{\Delta u}_m(n_k) = \frac{c_0 \widehat{\Delta\phi}_m(n_k)}{4\pi f_{dem}} = \frac{c_0}{4\pi f_{dem}} \angle r_{m,n}(\hat{D}(n_{k+1}) - \hat{D}(n_k), n_{k+1} - n_k), \tag{7}$$

where $|\ \widehat{D}(n_{k+1}) - \widehat{D}(n_k)\ | = 1$. The depth positions of correlation windows in the kth and $(k+1)$th key frames in (7) are different, whereas those in (4) are the same. This difference in the window positions corresponds to the compensation of global motion between these 2 key frames as shown in Fig. 4. Accumulated displacement $u_m(n_k)$ at depth $x_m(n_k)$ in the kth key frame is obtained by accumulation of the instantaneous displacement $\Delta u_m(n_k)$ during the period between 2 consecutive key frames as in (5).

$$\hat{u}_m(n_{k+1}) = \hat{u}_m(n_k) + \widehat{\Delta u}_m(n_k) \qquad (u_m(0) = 0). \tag{8}$$

In this procedure, it is only necessary to calculate the displacement $u_1(n)$ at the luminal interface for every 2 consecutive frames (nth and $(n+1)$th frames). For other points $\{m\}$, displacements $\{u_m(n_k)\}$ are calculated for every 2 consecutive key frames. This procedure significantly reduces the number of computations because there are multiple frames between 2 consecutive key frames.

2. Error Correcting Function: In the conventional method described in Section II-A, the frequency f_{dem} of the reference sinusoid in the quadrature demodulation is used

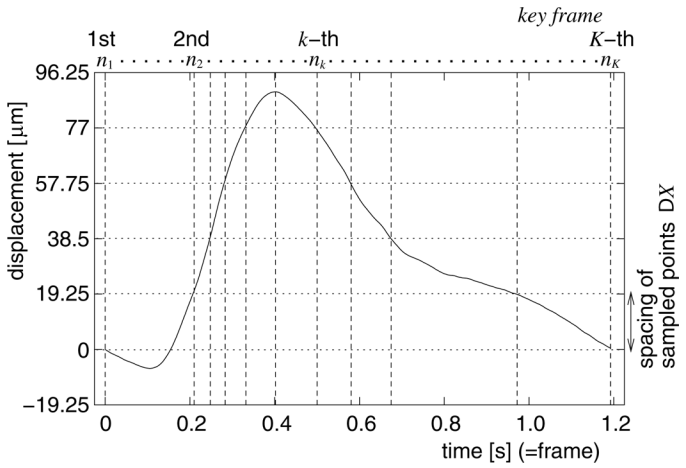

Fig. 3. Illustration of key frames.

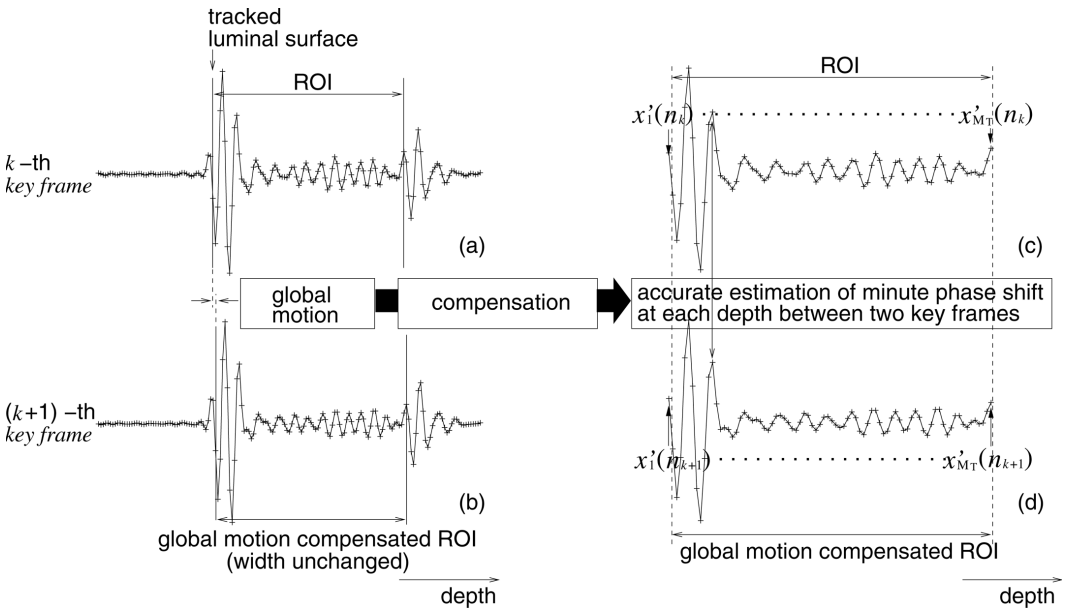

Fig. 4. Illustration of displacement estimation with global motion compensation.

instead of the actual center frequency $f_{c,m}(n)$, as shown in (4), to estimate the displacement $\Delta u_m(n)$. This assumption is also used in the modified method shown by (7). However, f_{dem} does not often match the actual center frequency $f_{c,m}(n)$ of the RF echo. Loupas *et al.* proposed a method for estimating the mean frequency, $\overline{f}_{c,m}(n)$, of the RF echo at each depth $x_m(n)$ in frame n [43]. In the method described in [43], [44], the estimated mean frequency

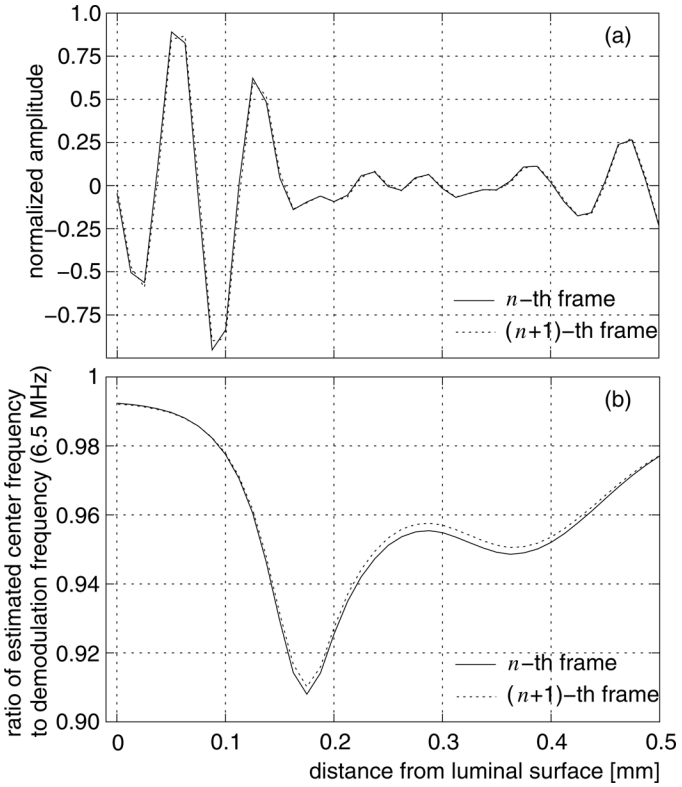

Fig. 5. (a) RF echoes and (b) center frequency distributions in 2 consecutive frames.

$\overline{f}_{c,m}(n)$ is used in (4) instead of the demodulation frequency f_{dem} to obtain an unbiased displacement estimate. The mean frequency, $\overline{f}_{c,m}(n)$, at the mth point in the nth frame is estimated as follows:

$$\overline{f}_{c,m}(n) = \overline{f}_{dem} - \frac{\angle r_{m,n}(1,0)}{2\pi T_s}, \tag{9}$$

where T_s is the sampling interval of the demodulated signal. By assuming that the mean frequency distributions $\{\overline{f}_{c,m}(n)\}$ $(m = 1,2,\ldots,M_T)$ in 2 consecutive frames are the same, the mean frequency distributions $\{\overline{f}_{c,m}(n)\}$ estimated by (9) are used in the estimation of instantaneous displacements $\{\Delta u_m(n)\}(m = 1,2,\ldots,M_T)$ between 2 consecutive frames.

Fig. 5(a) shows RF echoes from the phantom used in this study (the same as in Fig. 2) in 2 consecutive frames. The frame interval is 3.5 ms (= 1/286 Hz). Fig. 5(b) shows the ratio of the mean frequency $\overline{f}_{c,m}(n)$ estimated by (9) —M_c in (3) was set to 20—to the demodulation frequency f_{dem} of 6.5 MHz. There is a difference in the mean frequency distributions $\{\overline{f}_{c,m}(n)\}$ in 2 consecutive frames even though a high frame rate of 286 Hz was employed in this study.

Figs. 6(a) and 6(b) show RF echoes and mean frequency distributions estimated by (9) in 2 consecutive key frames. The interval between these 2 key frames is 69.9 ms. As shown in Fig. 6(b), there is a difference between the mean frequency distributions in 2 key frames. This difference is larger than that between 2 consecutive frames (3.5 ms) due to a longer frame interval.

In this study, an error correcting function, which does not require the assumption that the center frequency distributions in 2 different frames are the same, is introduced as follows: Let us consider the correlation functions

$r_{m,n_k}(0, n_{k+1} - n_k)$ and $r_{m,n_k}(\hat{D}(n_{k+1}) - \hat{D}(n_k), n_{k+1} - n_k)$ between 2 consecutive key frames. The absolute difference $\Delta d_m(n_k)$ between the displacements given by $\angle r_{0,n_k}(0, n_{k+1} - n_k)$ and $\angle r_{m,n_k}(\hat{D}(n_{k+1}) - \hat{D}(n_k), n_{k+1} - n_k)$ by substituting them into (4) instead of $\angle r_{m,n}(0,1)$ should be the spacing of sampled points ΔX because $|\hat{D}(n_{k+1}) - \hat{D}(n_k)| = 1$, i.e., the difference between the displacement estimated by the phase change of RF echo, which corresponds to $\widehat{\Delta d}_m(n_k)$, and the true displacement (corresponding to ΔX) is evaluated. Thus, the ratio $\gamma_m(n_k)$ of the estimated displacement difference $\widehat{\Delta d}_m(n_k)$ to the true displacement difference ($= \Delta X$) between the k-th and $(k+1)$th key frames is obtained as follows:

$$\gamma_m(n_k) = \frac{c_0}{4\pi f_{dem} \Delta X} \left| \angle r_{m,n_k}(0, n_{k+1} - n_k) - \angle r_{m,n_k}(\hat{D}(n_{k+1}) - \hat{D}(n_k), n_{k+1} - n_k) \right|. \tag{10}$$

By defining f_s as the sampling frequency of the demodulated signal, the numerator of (10) can be modified using the relation $\Delta X = c_0/(2f_s)$ as follows:

$$\begin{aligned}\gamma_m(n_k) &= \frac{c_0}{4\pi f_{dem} \cdot \frac{c_0}{2f_s}} \left| \angle \left\{ r^*_{m,n_k}(\hat{D}(n_{k+1}) - \hat{D}(n_k), n_{k+1} - n_k) \cdot r_{m,n_k}(0, n_{k+1} - n_k) \right\} \right| \\ &= \frac{f_s}{2\pi f_{dem}} \left| \angle \left\{ r^*_{m,n_k}(\hat{D}(n_{k+1}) - \hat{D}(n_k), n_{k+1} - n_k) \cdot r_{m,n_k}(0, n_{k+1} - n_k) \right\} \right|. \end{aligned} \tag{11}$$

Fig. 6(c) illustrates an example of the error correcting function $\gamma_m(n_k)$ for the RF signals shown in Fig. 6(a).

The error corrected displacement, $\widehat{\Delta u}_m(n_k)$, is obtained by using $\gamma_m(n_k)$ as the error correcting function as follows:

$$\widehat{\Delta u}_m(n_k) = \frac{1}{\gamma_m(n_k)} \frac{c_0}{4\pi f_{dem}} \angle r_{m,n_k}(\hat{D}(n_{k+1}) - \hat{D}(n_k), n_{k+1} - n_k). \tag{12}$$

C. Estimation of Radial Strain from the Displacement Distribution

Fig. 7(a) shows an example of a received RF echo. Fig. 7(b) shows an example of the estimated accumulated displacement, $\hat{u}_m$, at each sampled point m along an ultrasonic beam. Radial strain is obtained by estimating the regional slope of the displacement distribution $\{u_m\}$ ($m = 1,2,\ldots,M_T$). The regional slope, $\varepsilon_{r,m}$, around the mth sampled point (depth x_m) is estimated by minimizing the mean squared difference, α_m, between the measured regional displacements $\{\hat{u}_m\}$ and the linear model, $U_m = \varepsilon_{r,m} \cdot x + b_m$, as follows:

$$\alpha_m = \sum_{j=1}^{M_s} \left| \hat{u}_{m+j} - \varepsilon_{r,m} \cdot \Delta X \cdot j + b_m \right|^2 \quad (m \le M_T - M_s), \tag{13}$$

where M_s defines the width of region R for estimating the regional slope.

To obtain the strain distribution $\{\varepsilon_{r,m}\}$ in the direction of depth x, the region (layer) R in which the regional slope $\varepsilon_{r,m}$ is estimated is slid in the direction of depth x along an ultrasonic beam by intervals of the sampled points. Therefore, several layers overlap at the mth sampled point because the layer thickness $M_s \cdot \Delta X$ is greater than the interval ΔX of the sampled points. Thus, the compounded

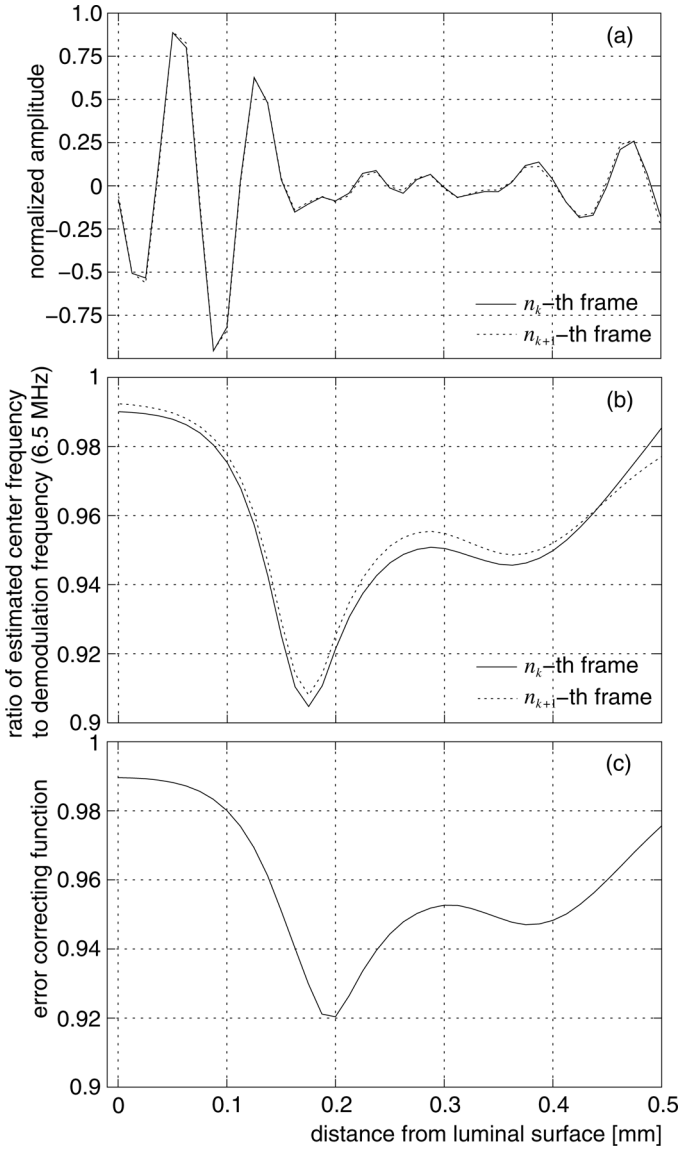

Fig. 6. (a) RF echoes and (b) center frequency distributions in 2 consecutive key frames; (c) error correcting function $\gamma_m(n_k)$.

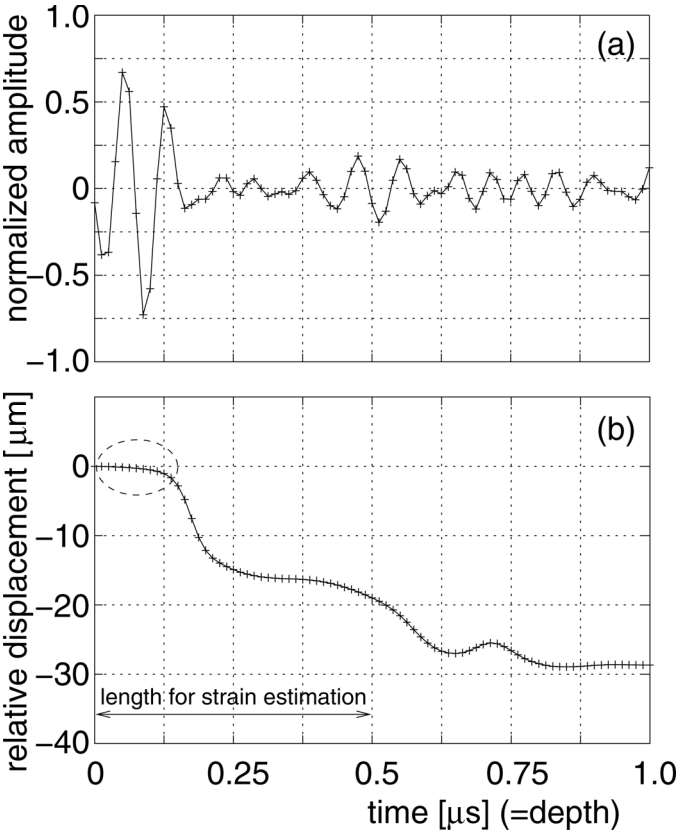

Fig. 7. Illustration of strain estimation: (a) RF echo from the posterior wall of the phantom used in this study and (b) displacement distribution along an ultrasonic beam.

radial strain, $\bar{\varepsilon}_{r,m}$ [45], at the mth sampled point is obtained by simply averaging the estimated regional slopes $\hat{\varepsilon}_{r,m}$ of the layers, which overlap at the mth point as follows:

$$\bar{\varepsilon}_{r,m} = \begin{cases} \dfrac{1}{L_m}\displaystyle\sum_{j=1}^{L_m} \hat{\varepsilon}_{r,m-j+1} & (m \le M_T - M_s), \\ \dfrac{1}{L_m}\displaystyle\sum_{j=1}^{L_m} \hat{\varepsilon}_{r,M_T-M_s-j+1} & (m > M_T - M_s), \end{cases} \tag{14}$$

where L_m is the number of overlapping layers at the mth point.

As shown in Fig. 7(a), a dominant echo from the luminal interface is found in the period from 0 to about 0.13 μs. The phase shift of sampled points within this echo corresponds to the displacement of the luminal interface. Therefore, a constant displacement is found during the duration of that echo as shown by the region surrounded by the dashed line in Fig. 7(b). As a result, strain is hardly detected during that period (from 0 to 0.13 μs) when the width M_s for estimation of the regional slope in (13) is less than the pulse duration. However, such a decrease in the estimated strain is just an artifact due to the finite pulse duration. To reduce this artifact, in this study, the width used for estimating the regional slope $\varepsilon_{r,m}$ was set to be longer than the duration of the employed ultrasonic pulse.

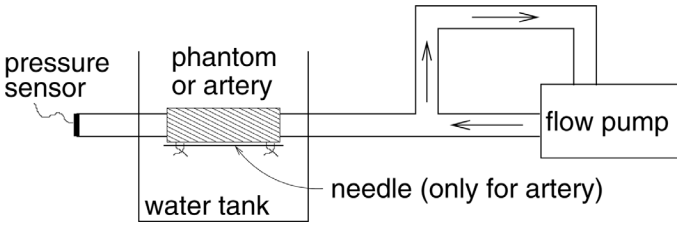

Fig. 8. Schematic diagram of measurement system.

III. Materials and Methods

In this study, a cylindrical phantom and an excised artery were measured by ultrasound. The outer and inner diameters of the phantom, made of silicone rubber, were 10 and 8 mm, respectively. The phantom contained 5% carbon powder (by weight) to obtain sufficient scattering from inside the wall.

Fig. 8 shows a schematic diagram of the measurement system. A change in pressure inside the phantom or artery was induced by circulating a fluid using a flow pump. The change in internal pressure was measured by a pressure sensor (9E02-P16, NEC, Tokyo, Japan).

In ultrasonic measurement, the phantom and artery were measured with a linear-type ultrasonic probe (SSD-6500, Aloka, Tokyo, Japan). The nominal center frequency was 10 MHz. RF echoes were acquired at 40 MHz at a frame rate of 286 Hz.

Pressure-diameter testing was applied to the phantom to obtain the elastic modulus of silicone rubber. In the pressure-diameter testing, the change in external diameter of the phantom was measured with a laser line gauge (VG-035, KEYENCE, Osaka, Japan).

In the *in vitro* experiment, a femoral artery excised from a patient with arteriosclerosis obliterans was measured. The artery was placed in a water tank filled with 0.9% saline solution at room temperature. A needle was attached to the external surface of the posterior wall using strings to identify the sections to be imaged during the ultrasonic measurement. After the ultrasonic measurement, pathological images of the measured sections were obtained with reference to the needle.

IV. Basic Experimental Results

A. Pressure-Diameter Testing of the Phantom

Fig. 9(a) shows the trigger signal for driving the flow pump. Figs. 9(b) and 9(c) show waveforms of the internal pressure and change in the external diameter of the phantom, respectively. In Fig. 9, the waveforms of 10 measurements are superimposed. From the measured internal pressure, p_i, and the change in external diameter, $2{\cdot}\Delta r_o$, the elastic modulus, E, is obtained as follows [46]:

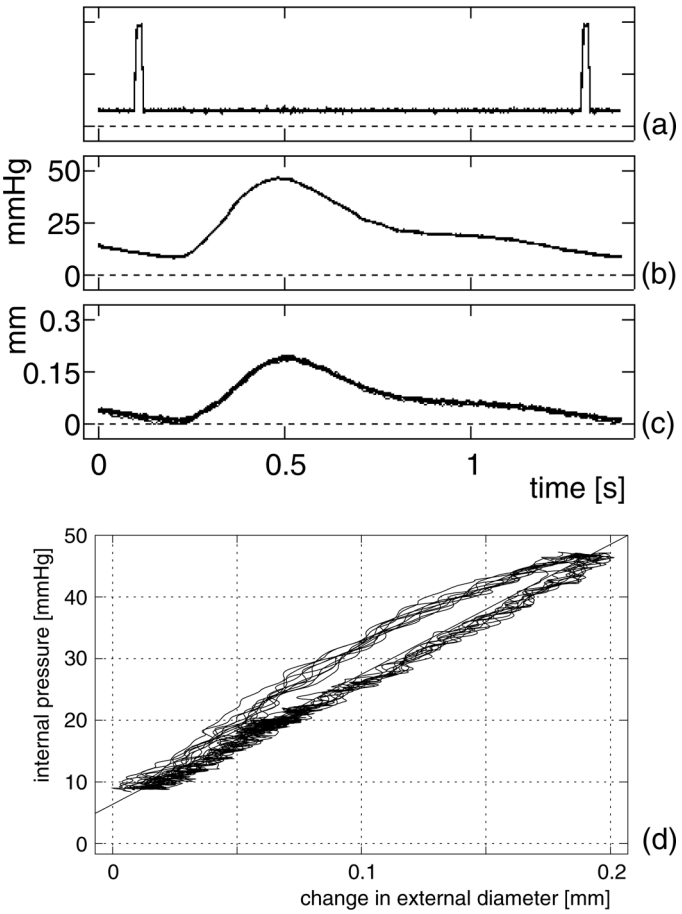

Fig. 9. Waveforms of internal pressure p_i and change in external diameter $2\Delta r_o$ of the phantom: (a) trigger signal for the flow pump; (b) internal pressure p_i; (c) change in external diameter $2\Delta r_o$; and (d) relationship between internal pressure p_i and change in external diameter $2\Delta r_o$ of the phantom.

$$E = \frac{3}{2}\frac{r_i^2}{r_o^2 - r_i^2}\frac{p_i}{\varepsilon_\theta} = \frac{3}{2}\frac{r_i^2}{r_o^2 - r_i^2}\frac{p_i}{\frac{\Delta r_o}{r_o}} = \frac{3}{2}\frac{r_i^2 r_o}{r_o^2 - r_i^2}\frac{p_i}{\Delta r_o}, \tag{15}$$

where r_i and r_o are the original internal and external radii, respectively.

In Fig. 9(d), the measured internal pressure p_i is plotted as a function of the change in external diameter $2\Delta r_o$. The slope, $p_i/\Delta r_o$, was estimated by applying the least-squares method to the measured data shown in Fig. 9(d). The estimated slope $p_i/\Delta r_o$ is shown by the solid line in Fig. 9(d). The elastic modulus E of the phantom was determined to be 749 kPa.

B. Ultrasonic Measurements of the Phantom

1. Comparison of Conventional and Proposed Methods: The radial strain distribution inside the wall of the phantom was estimated by the conventional phase-sensitive correlation method described in Section II-A, as shown in Fig. 10(a). In this section, the length of the correlation window determined by M_c and that for estimating strain determined by M_s are set to 0.5 μs (corresponding to the length at −20 dB of the maximum magnitude of the quadrature demodulated signal of the ultrasonic pulse, $M_c = 20$) and 1.0 μs (twice the length at −20 dB, $M_s = 40$), respectively, for both the conventional and proposed methods. In Fig. 10(a), plots and vertical bars show the means and standard deviations of the radial strain in the radial direction (along the ultrasonic beam). The mean value and standard deviation at each radial position are obtained by the individual strain distributions along 46 ultrasonic beams. The solid curve in Fig. 10(a) shows the theoretical radial strain ε_r of a homogeneous tube at each radial position r, which is obtained using the elastic modulus E measured by pressure-diameter testing and the measured internal pressure as follows [46]:

$$\varepsilon_r = -\frac{3}{2}\frac{r_i^2 r_o^2}{(r_o^2 - r_i^2)r^2}\frac{p_i}{E}. \tag{16}$$

In Fig. 10(a), mean values tend to follow the theoretical profile. However, the standard deviation is large. Mean error e_{mean} and standard deviation SD_{mean} evaluated by (17) and (18) were 23.7% and 46.2%, respectively.

$$e_{\text{mean}} = \frac{1}{M_T}\sum_{m=1}^{M_T}\frac{\left|E_i[\hat{\varepsilon}_{m,i}] - \varepsilon_{r=x_m}\right|}{\left|\varepsilon_{r=x_m}\right|}, \tag{17}$$

$$\text{SD}_{\text{mean}} = \frac{1}{M_T}\sum_{m=1}^{M_T}\frac{\sqrt{E_i[(\hat{\varepsilon}_{m,i} - E[\hat{\varepsilon}_{m,i}])^2]}}{\left|\varepsilon_{r=x_m}\right|}, \tag{18}$$

where $E_i[\cdot]$ represents the averaging with respect to the beam position i.

Fig. 10(b) shows the strain distribution obtained by the conventional phase-sensitive correlation method with mean frequency estimation (Loupas's method) [43]. There is no distinct improvement in the strain estimates. The strain distribution obtained by Loupas's method with spatial compounding [45] shown in Fig. 10(c) is in good agreement with the theoretical strain profile, and the standard deviation is significantly reduced. Note that vertical scales in Figs. 10(c) and 10(d) are different from those in Figs. 10(a) and 10(b).

Fig. 10(d) shows the radial strain distribution obtained by the method proposed in this study. The difference between the mean values and the theoretical profile shown by the solid curve was further reduced, but the standard deviation was similar to that obtained by Loupas's method with spatial compounding. From this result, it can be said that the variance was reduced mainly by the spatial compounding. Mean error e_{mean} and standard deviation SD_{mean} of the strain distribution estimated by the proposed method were $e_{\text{mean}} = 12.0\%$ and $\text{SD}_{\text{mean}} = 14.1\%$, respectively.

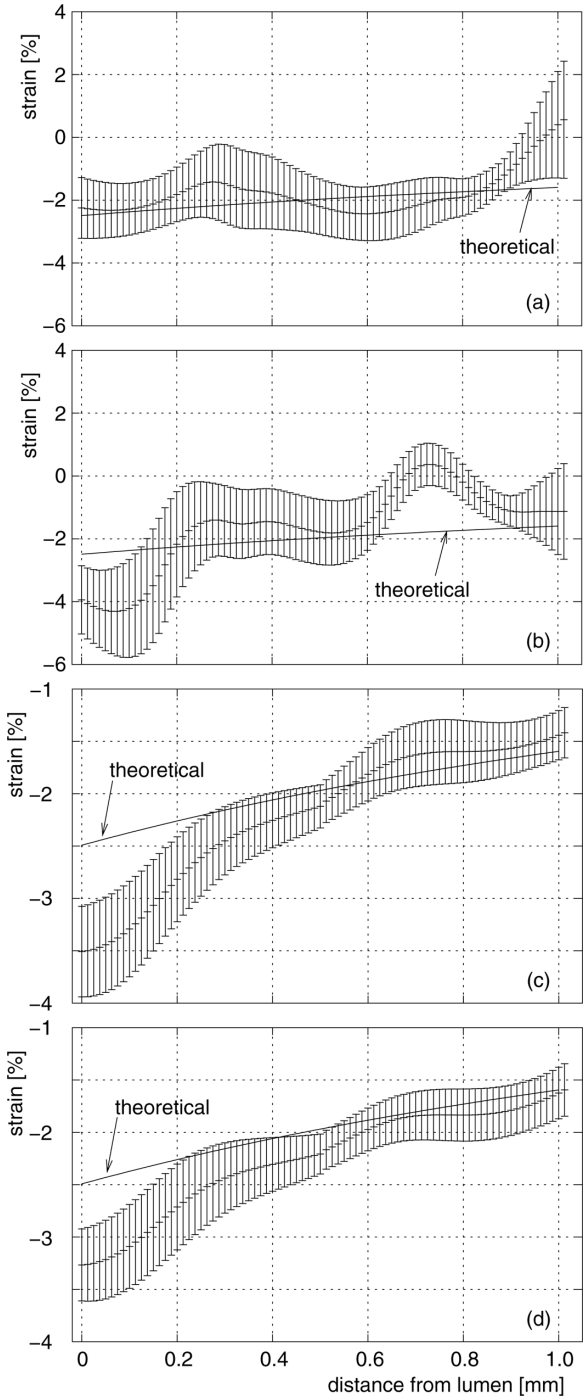

Fig. 10. Radial strain distributions of the phantom obtained by (a) conventional phase-sensitive correlation method (phased-tracking method) [23]; (b) conventional phase-sensitive correlation method with mean frequency estimation (Loupas's method) [43]; (c) Loupas's method with spatial compounding [45]; and (d) proposed method.

2. Consideration of the Size of Correlation Window and Period for Estimating Strain: Fig. 11(a) shows error e_{mean} in the strain distribution of the phantom estimated by the proposed method at each combination of the period for estimating strain and the length of the correlation window. As shown in Fig. 11, error e_{mean} is reduced by lengthening the period for estimating strain, and this effect of error reduction is almost complete at 1.0 μs ($M_s = 40$ in (13)).

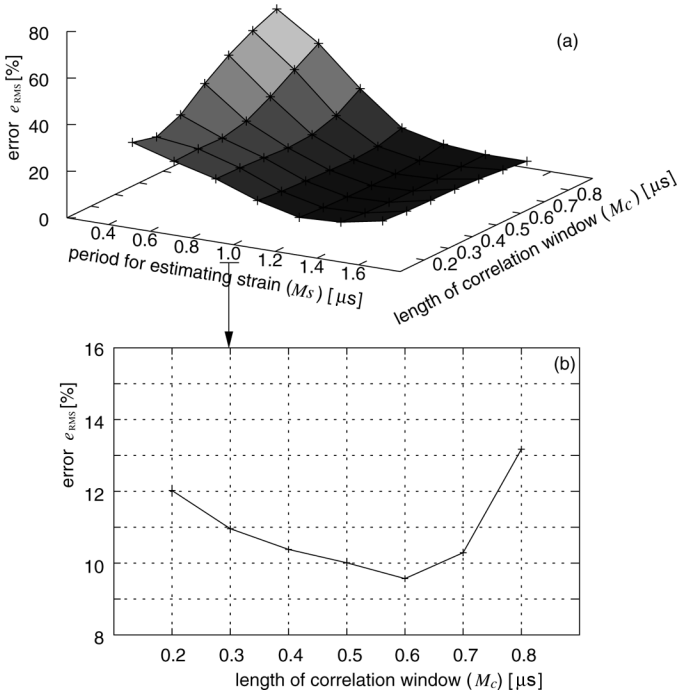

Fig. 11. Error in the strain distribution estimated by the proposed method: (a) error at each combination of the period for estimating strain, M_s in (13), and length of correlation window, M_c in eq. (3); (b) error distribution at the period for estimating strain of 1.0 μs.

Fig. 11(b) shows the error distribution at the period for estimating strain of 1.0 μs. The strain estimates are not much influenced by the correlation window length in comparison with the period for strain estimation, and the error reduction is almost complete at the correlation window lengths of 0.5 μs. Therefore, the length of 0.5 μs ($M_c = 20$ in (3) and (7)) was selected to achieve a better spatial resolution, whereas the error at 0.6 μs is slightly smaller. The correlation window length of 0.5 μs ($M_c = 20$) and the period for estimating strain of 1.0 μs ($M_s = 40$) correspond to the length at −20 dB of the maximum magnitude of the quadrature demodulated signal of the ultrasonic pulse and twice that length, respectively.

V. *In Vitro* Experimental Results

Figs. 12(a-1) and 12(b-1) show the B-mode images of 2 different regions in the excised femoral artery. The region shown in Fig. 12(a-2) shows very low strain. On the other hand, the region shown in Fig. 12(b-2) shows relatively larger strain, and there is a clear strain decay with respect to the distance from the lumen [46]. Figs. 12(a-3) and 12(b-3) show the elasticity images obtained by (16) using the measured internal pressure and estimated strain distributions. By comparing the elasticity images and pathological images of the corresponding sections shown in Figs. 12(a-4), 12(b-4), 12(a-5), and 12(b-5), the very hard region surrounded by the green line in Fig. 12(a-3) corresponds to calcified tissue. On the other hand, the region composed of smooth muscle and collagen shows a relatively homogeneous and lower elastic modulus dis-

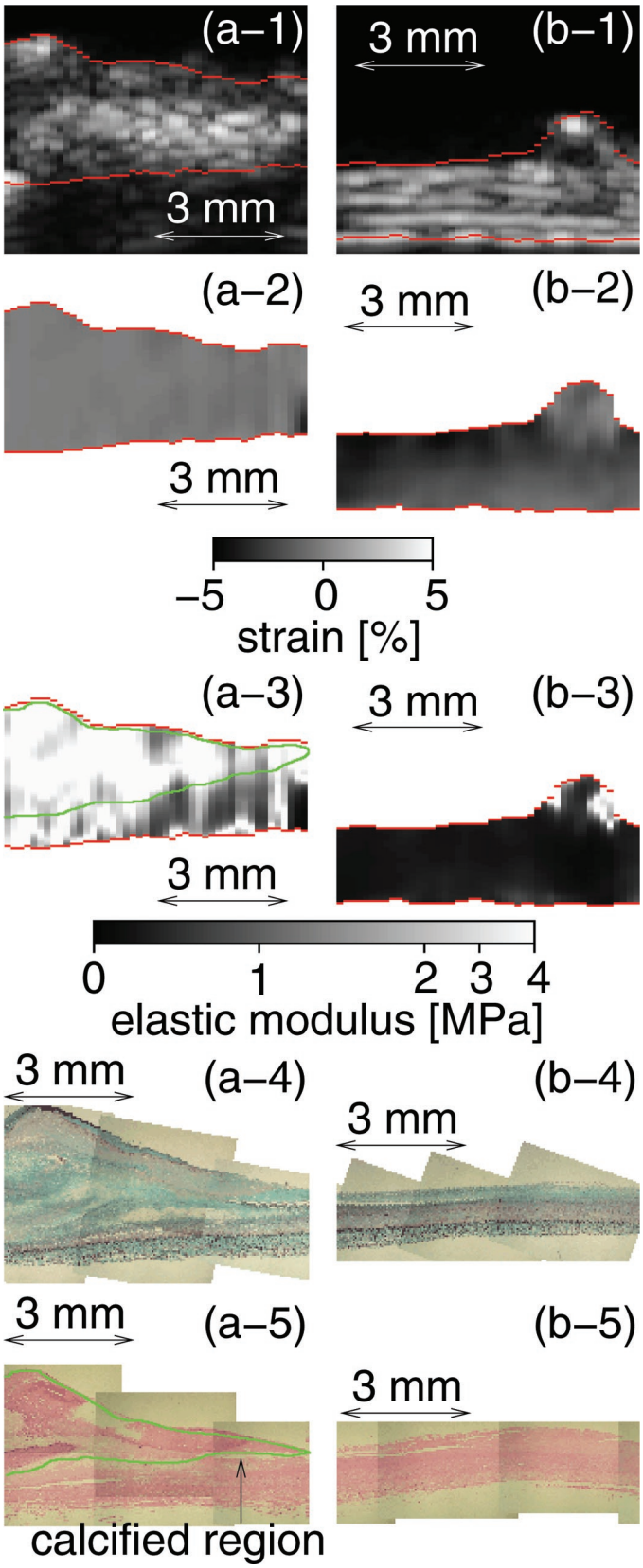

Fig. 12. *In vitro* experimental results for 2 regions: (a) that with calcified tissue and (b) that without calcified tissue and composed of smooth muscle and collagen; (1) B-mode images, (2) strain images, (3) elasticity images, and (4) and (5) pathological images with elastica-Masson and hematoxilin-eosin staining, respectively.

tribution. These results show that the proposed method successfully reveals the difference in the deformation properties resulting from different tissue compositions.

VI. Discussion

In the method proposed in this study, the interval of frames between which the phase shift of echoes is estimated was increased to reduce the number of computations. However, aliasing does not occur because the large global motion is tracked (compensated) by the conventional method at a high frame rate of 286 Hz. The global motion between 2 key frames is the distance corresponding to an interval of sampled points, 19.25 μm in this study (speed of sound: 1,540 m/s). Therefore, the residual displacements at other radial positions after global motion compensation are less than 19.25 μm after global motion compensation. When the center frequency of the received RF echo is exactly the same as the nominal center frequency (10 MHz) of the employed ultrasonic probe, a displacement of 19.25 μm produces a phase shift of RF echoes of $\pi/2$. The residual displacement at each radial position after global motion compensation is smaller than 19.25 μm, which is smaller than the aliasing limit of 38.5 μm at 10 MHz.

The proposed method does not remove the global motion perfectly because the displacement at the luminal interface estimated by the conventional phase-sensitive correlation method is used to compensate for the global motion, and, in usual cases, the frequency of the reference sinusoid used in the quadrature demodulation does not exactly match the center frequency of the RF echo from the luminal interface. However, even in such situations, the proposed method can compensate for most of the global motion, and it is one of the simplest ways to track the global motion.

On the other hand, by using companding to find the exact match between the precompression and postcompression RF signals [11], [12], [35]–[40], more accurate displacement estimates would be achieved because such methods do not require information on the center frequency and enable better correction of the difference between the center frequencies of 2 RF signals. In the present study, however, RF signals were sampled at a frequency only 4 times the transmit center frequency, whereas a higher sampling frequency (or interpolation) is desirable in such other methods. The objective of this study was to develop a method that can be applied to an RF signal sampled at a lower frequency with less computation but reasonable accuracy, and the scientific meaning of this study is the introduction of an error correcting function that reduces the influence of the center frequency variation on the displacement estimation without requirement of the assumption that the center frequency distributions in 2 different frames are the same.

As described above, in this study, improvement of the strain estimates by the proposed method was shown by basic experiments using a cylindrical phantom. The true

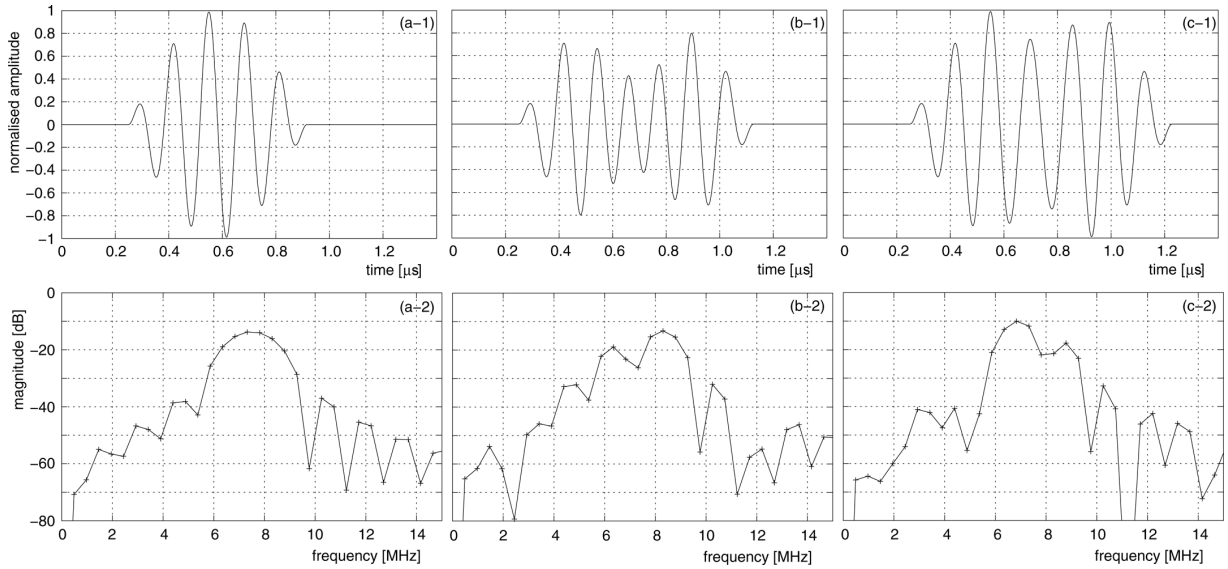

Fig. 13. RF echoes and their power spectra (center frequency: 7.5 MHz): (a) from a single scatterer; (b) from 2 scatterers with a spacing of 162 μm; and (c) from 2 scatterers with a spacing of 240 μm.

strain distribution in an actual arterial wall is difficult to know, particularly in the case of a diseased region, as shown in Fig. 12(a). Therefore, in this study, we just demonstrated that the strain and elasticity distributions estimated by the proposed method were in good agreement with the pathology. The usefulness of the proposed method in clinical situations should be further investigated by applying it to more arteries in *in vitro* and *in vivo* experiments.

Finally, in the estimation of the elastic modulus, determination of the stress distribution is a major problem. In this study, the stress distribution defined by (16) was used to obtain the elasticity images shown in Fig. 12(a-3) and 12(b-3). However, it agrees with the actual stress distribution only in the case of a homogeneous cylindrical shell. Such a difference between the actual stress distribution and that used in elasticity estimation leads to a significant error. Recently, several studies have been conducted to reconstruct elastic modulus distributions [47]–[49]. However, the method employed has not yet been applied to both longitudinal and cross-sectional scans of the arteries, and determination of the stress distribution remains an important problem in vascular elasticity imaging.

VII. Conclusions

In the displacement estimation based on the phase change of echoes, the displacement estimates are biased when the center frequency of the RF echo changes. Such an apparent change in the center frequency could be caused by the interference of echoes from scatterers. To reduce the influence of the center frequency variation on the estimation of artery-wall strain, in this study, an error correcting function, which does not require the assumption that the center frequency distributions in 2 different frames are the same, was introduced. As a result, the proposed method provides better strain estimates in comparison with conventional phase-sensitive correlation methods.

Appendix
Influences of Interference on Center Frequency

In the case of a target containing multiple scatterers, the interference between echoes from these scatterers occurs because there are multiple scatterers within the duration of an ultrasonic pulse. An ultrasonic pulse has a certain frequency bandwidth, and thus the interference of echoes could be one of the reasons for the change in center frequency.

Fig. 13(a-1) shows a simulated RF echo from a single point scatterer, and Fig. 13(a-2) shows its power spectrum. The center frequency is set to 7.5 MHz, and the envelope is a Hanning window with a length corresponding to 5 cycles of the center frequency. Figs. 13(b-1) and 13(c-1) show the RF echoes from 2 scatterers that exist along an ultrasonic beam. The spacings of scatterers in Figs. 13(b-1) and 13(c-1) are 162 μm and 240 μm, respectively. As shown in Figs. 13(a-2), 13(b-2), and 13(c-2), depending on the spacing of scatterers, even when there are only 2 scatterers, the dominant frequency changes in a complex way due to the interference of echoes.

Acknowledgments

We are grateful to Panasonic Co., Ltd. for providing the phantoms used in this study. This work was supported by the Ministry of Education, Science, Sports and Culture and was partly supported by the Suzuken Memorial Foundation.

References

[1] R. T. Lee, A. J. Grodzinsky, E. H. Frank, R. D. Kamm, and F. J. Schoen, "Structure-dependent dynamic mechanical behavior of fibrous caps from human atherosclerotic plaques," *Circulation*, vol. 83, no. 5, pp. 1764–1770, 1991.

[2] H. M. Loree, A. J. Grodzinsky, S. Y. Park, L. J. Gibson, and R. T. Lee, "Static circumferential tangential modulus of human atherosclerotic tissue," *J. Biomech.*, vol. 27, no. 2, pp. 195–204, 1994.

[3] M. Benthin, P. Dahl, R. Ruzicka, and K. Lindström, "Calculation of pulse-wave velocity using cross-correlation–effects of reflexes in the arterial tree," *Ultrasound Med. Biol.*, vol. 17, no. 5, pp. 461–469, 1991.

[4] H. Kanai, K. Kawabe, M. Takano, R. Murata, N. Chubachi, and Y. Koiwa, "New method for evaluating local pulse wave velocity by measuring vibrations on aortic wall," *Electron. Lett.*, vol. 30, no. 7, pp. 534–536, 1993.

[5] P. J. Brands, J. M. Willigers, L. A. F. Ledoux, R. S. Reneman, and A. P. G. Hoeks, "A noninvasive method to estimate pulse wave velocity in arteries locally by means of ultrasound," *Ultrasound Med. Biol.*, vol. 24, no. 9, pp. 1325–1335, 1998.

[6] A. Eriksson, E. Greiff, T. Loupas, M. Persson, and P. Pesque, "Arterial pulse wave velocity with tissue Doppler imaging," *Ultrasound Med. Biol.*, vol. 28, no. 5, pp. 571–580, 2002.

[7] J. M. Meinders, P. J. Brands, J. M. Willigers, L. Kornet, and A. P. G. Hoeks, "Assessment of the spatial homogeneity of artery dimension parameters with high frame rate 2-D B-mode," *Ultrasound Med. Biol.*, vol. 27, no. 6, pp. 785–794, 2001.

[8] A. P. G. Hoeks, C. J. Ruissen, P. Hick, and R. S. Reneman, "Transcutaneous detection of relative changes in artery diameter," *Ultrasound Med. Biol.*, vol. 11, no. 1, pp. 51–59, 1985.

[9] T. Länne, H. Stale, H. Bengtsson, D. Gustafsson, D. Bergqvist, B. Sonesson, H. Lecerof, and P. Dahl, "Noninvasive measurement of diameter changes in the distal abdominal aorta in man," *Ultrasound Med. Biol.*, vol. 18, no. 5, pp. 451–457, 1992.

[10] P. J. Brands, A. P. G. Hoeks, M. C. M. Rutten, and R. S. Reneman, "A noninvasive method to estimate arterial impedance by means of assessment of local diameter change and the local center-line blood flow velocity using ultrasound," *Ultrasound Med. Biol.*, vol. 22, no. 7, pp. 895–905, 1996.

[11] J. Ophir, I. Céspedes, H. Ponnekanti, Y. Yazdi, and X. Li, "Elastography: A quantitative method for imaging the elasticity of biological tissues," *Ultrason. Imag.*, vol. 13, pp. 111–134, 1991.

[12] I. Céspedes and J. Ophir, "Reduction of image noise in elastography," *Ultrason. Imag.*, vol. 15, pp. 89–102, 1993.

[13] E. E. Konofagou, J. Ophir, T. Varghese, and F. Kallel, "A new elastographic method for estimation and imaging of lateral displacements, lateral strains, corrected axial strain and Poisson's ratios in tissues," *Ultrasound Med. Biol.*, vol. 24, no. 8, pp. 1183–1199, 1998.

[14] J. Ophir, B. Garra, F. Kallel, E. Konofagou, T. Krouskop, R. Righetti, and T. Varghese, "Elastographic imaging," *Ultrasound Med. Biol.*, vol. 26, pp. S23–S29, 2000.

[15] C. L. de Korte, E. I. Céspedes, A. F. W. van der Steen, and C. T. Lanée, "Intravascular elasticity imaging using ultrasound: Feasibility studies in phantoms," *Ultrasound Med. Biol.*, vol. 23, no. 5, pp. 735–746, 1997.

[16] E. I. Céspedes, C. L. de Korte, and A. F. W. van der Steen, "Intraluminal ultrasonic palpation: Assessment of local and cross-sectional tissue stiffness," *Ultrasound Med. Biol.*, vol. 26, no. 3, pp. 385–396, 2000.

[17] O. Bonnefous, "Blood flow and tissue motion with ultrasound for vascular applications," *C. R. Acad. Sci. Ser. IV Phys.*, vol. 2, pp. 1161–1178, 2001.

[18] R. L. Maurice, J. Ohayon, Y. Frétigny, M. Bertrand, G. Soulez, and G. Cloutier, "Noninvasive vascular elastography: Theoretical framework," *IEEE Trans. Med. Imag.*, vol. 23, no. 2, pp. 164–180, 2004.

[19] H. Ribbers, S. Holewijn, J. D. Blankensteijn, and C. L. de Korte, "Non-invasive two dimensional elastography of the carotid artery," in *Proc. 2005 IEEE Ultrasonics Symp.*, pp. 1113–1116.

[20] K. Kim, W. F. Weitzel, J. M. Rubin, H. Xie, X. Chen, and M. O'Donnell, "Vascular intramural strain imaging using arterial pressure equalization," *Ultrasound Med. Biol.*, vol. 30, no. 6, pp. 761–771, 2004.

[21] M. A. Lubinski, S. Y. Emelianov, and M. O'Donnell, "Speckle tracking methods for ultrasonic elasticity imaging using short-time correlation," *IEEE Trans. Ultrason. Ferroelectr. Freq. Control*, vol. 46, no. 1, pp. 82–96, 1999.

[22] E. Brusseau, J. Fromageau, G. Finet, P. Delachartre, and D. Vray, "Axial strain imaging of intravascular data: Results on polyvinyl alcohol cryogel phantoms and carotid artery," *Ultrasound Med. Biol.*, vol. 27, no. 12, pp. 1631–1642, 2001.

[23] H. Kanai, M. Sato, Y. Koiwa, and N. Chubachi, "Transcutaneous measurement and spectrum analysis of heart wall vibrations," *IEEE Trans. Ultrason. Ferroelectr. Freq. Control*, vol. 43, no. 5, pp. 791–810, 1996.

[24] H. Hasegawa, H. Kanai, Y. Koiwa, and N. Chubachi, "Noninvasive evaluation of Poisson's ratio of arterial wall using ultrasound," *Electron. Lett.*, vol. 33, no. 4, pp. 340–342, 1997.

[25] H. Kanai, H. Hasegawa, N. Chubachi, Y. Koiwa, and M. Tanaka, "Noninvasive evaluation of local myocardial thickening and its color-coded imaging," *IEEE Trans. Ultrason. Ferroelectr. Freq. Control*, vol. 44, no. 4, pp. 752–768, 1997.

[26] H. Kanai, Y. Koiwa, and J. Zhang, "Real-time measurements of local myocardium motion and arterial wall thickening," *IEEE Trans. Ultrason. Ferroelectr. Freq. Control*, vol. 46, no. 5, pp. 1229–1241, 1999.

[27] H. Hasegawa, H. Kanai, and Y. Koiwa, "Modified phased tracking method for measurement of change in thickness of arterial wall," *Jpn. J. Appl. Phys.*, vol. 41, no. 5B, pp. 3563–3571, 2002.

[28] H. Hasegawa, H. Kanai, N. Hoshimiya, and Y. Koiwa, "Evaluating the regional elastic modulus of a cylindrical shell with nonuniform wall thickness," *J. Med. Ultrason.*, vol. 31, no. 2, pp. 81–90, 2004.

[29] H. Kanai, H. Hasegawa, M. Ichiki, F. Tezuka, and Y. Koiwa, "Elasticity imaging of atheroma with transcutaneous ultrasound–preliminary study," *Circulation*, vol. 107, no. 24, pp. 3018–3021, 2003.

[30] J. Inagaki, H. Hasegawa, H. Kanai, M. Ichiki, F. Tezuka, and Y. Koiwa, "Construction of reference data for tissue characterization of arterial wall based on elasticity images," *Jpn. J. Appl. Phys.*, vol. 44, no. 6B, pp. 4593–4597, 2005.

[31] J. Inagaki, H. Hasegawa, H. Kanai, M. Ichiki, F. Tezuka, and Y. Koiwa, "Tissue classification of arterial wall based on elasticity image," *Jpn. J. Appl. Phys.*, vol. 45, no. 5B, pp. 4732–4735, 2006.

[32] C. Kasai, K. Namekawa, A. Koyano, and R. Omoto, "Real-time two-dimensional blood flow imaging using an autocorrelation technique," *IEEE Trans. Sonics Ultrason.*, vol. SU-32, no. 3, pp. 458–464, 1985.

[33] E. E. Konofagou, T. Varghese, J. Ophir, and S. K. Alam, "Power spectral strain estimators in elastography," *Ultrasound Med. Biol.*, vol. 25, no. 7, pp. 1115–1129, 1999.

[34] E. E. Konofagou, T. Varghese, and J. Ophir, "Spectral estimators in elastography," *Ultrasonics*, vol. 38, pp. 412–416, 2000.

[35] J. W. Betz, "Comparison of the deskewed short-time correlator and the maximum likelihood correlator," *IEEE Trans. Acoust. Speech Signal Process.*, vol. ASSP-32, no. 2, pp. 285–294, 1984.

[36] J. C. Hassab, B. W. Guimond, and S. C. Nardone, "Estimation of location and motion parameters of a moving source observed from a linear array," *J. Acoust. Soc. Am.*, vol. 70, no. 4, pp. 1054–1061, 1981.

[37] W. B. Adams, J. P. Kuhn, and W. P. Whyland, "Correlation compensation requirements for passive time delay estimation with moving source or receivers," *IEEE Trans. Acoust. Speech Signal Process.*, vol. ASSP-28, no. 2, pp. 158–168, 1980.

[38] M. Bilgen and M. F. Insana, "Deformation models and correlation analysis in elastography," *J. Acoust. Soc. Am.*, vol. 99, no. 5, pp. 3212–3224, 1996.

[39] T. Varghese and J. Ophir, "Performance optimization in elastography: Multicompression with temporal stretching," *Ultrason. Imag.*, vol. 18, pp. 193–214, 1996.

[40] S. K. Alam and J. Ophir, "Reduction of signal decorrelation from mechanical compression of tissues by temporal stretching: Applications to elastography," *Ultrasound Med. Biol.*, vol. 23, no. 2, pp. 95–105, 1997.

[41] T. Varghese and J. Ophir, "Enhancement of echo-signal correlation in elastography using temporal stretching," *IEEE Trans. Ultrason. Ferroelectr. Freq. Control*, vol. 44, no. 1, pp. 173–180, 1997.

[42] S. K. Alam, J. Ophir, and E. E. Konofagou, "An adaptive strain estimator for elastography," *IEEE Trans. Ultrason. Ferroelectr. Freq. Control*, vol. 45, no. 2, pp. 461–472, 1998.

[43] T. Loupas, J. T. Powers, and R. W. Gill, "An axial velocity estimator for ultrasound blood flow imaging, based on a full evaluation of the Doppler equation by means of a two-dimensional autocorrelation approach," *IEEE Trans. Ultrason. Ferroelectr. Freq. Control*, vol. 42, no. 4, pp. 672–688, 1995.

[44] S. I. Rabben, S. Bjærum, V. Sørhus, and H. Torp, "Ultrasound-based vessel wall tracking: An auto-correlation technique with RF center frequency estimation," *Ultrasound Med. Biol.*, vol. 28, no. 4, pp. 507–517, 2002.
[45] H. Hasegawa and H. Kanai, "Modification of the phased-tracking method for reduction of artifacts in estimated artery wall deformation," *IEEE Trans. Ultrason. Ferroelectr. Freq. Control*, vol. 53, no. 11, pp. 2050–2064, 2006.
[46] S. P. Timoshenko and J. N. Goodier, *Theory of Elasticity*, 3rd ed. New York: McGraw Hill, 1970.
[47] R. A. Baldewsing, F. Mastik, J. A. Schaar, P. W. Serruys, and A. F. W. van der Steen, "Young's modulus reconstruction of vulnerable atherosclerotic plaque components using deformable curves," *Ultrasound Med. Biol.*, vol. 32, no. 2, pp. 201–210, 2006.
[48] R. A. Baldewsing, J. A. Shaar, F. Mastik, C. W. J. Oomens, and A. F. W. van der Steen, "Assessment of vulnerable plaque composition by matching the deformation of a parametric plaque model to measured plaque deformation," *IEEE Trans. Med. Imaging*, vol. 24, no. 4, pp. 514–528, 2005.
[49] R. A. Baldewsing, C. L. de Korte, J. A. Shaar, F. Mastik, and A. F. W. van der Steen, "A finite element model for performing intravascular ultrasound elastography of human atherosclerotic coronary arteries," *Ultrasound Med. Biol.*, vol. 30, no. 6, pp. 803–813, 2004.

Hideyuki Hasegawa was born in Oyama, Japan, in 1973. He received the B.E. degree from Tohoku University, Sendai, Japan, in 1996. He received the Ph.D. degree from Tohoku University in 2001. He is presently an associate professor in Graduate School of Engineering, Tohoku University.

His main research interest is medical ultrasound, especially diagnosis of atherosclerosis based on measurement of mechanical properties of the arterial wall.

Dr. Hasegawa is a member of the IEEE, the Acoustical Society of Japan, the Japan Society of Ultrasonics in Medicine, and the Institute of Electronics, Information and Communication Engineers.

Hiroshi Kanai (M'98) was born in Matsumoto, Japan, on November 29, 1958. He received a B.E. degree from Tohoku University, Sendai, Japan in 1981, and M.E. and the Ph. D. degrees, also from Tohoku University, in 1983 and in 1986, both in Electrical Engineering.

From 1986 to 1988 he was with the Education Center for Information Processing, Tohoku University, as a research associate. From 1990 to 1992 he was a lecturer in the Department of Electrical Engineering, Faculty of Engineering, Tohoku University. From 1992 to 2001 he was an associate professor in the Department of Electrical Engineering, Faculty of Engineering, Tohoku University. Since 2001 he has been a professor in the Department of Electronic Engineering, Graduate School of Engineering, Tohoku University.

His present interests are in ultrasonic measurement and digital signal processing for diagnosis of heart diseases and arteriosclerosis.

Dr. Kanai is a member of the Acoustical Society of Japan, the Institute of Electronics Information and Communication Engineering of Japan, the Japan Society of Ultrasonics in Medicine, Japan Society of Medical Electronics and Biological Engineering, and the Japanese Circulation Society.